Chapter 1

Motivations and opportunities

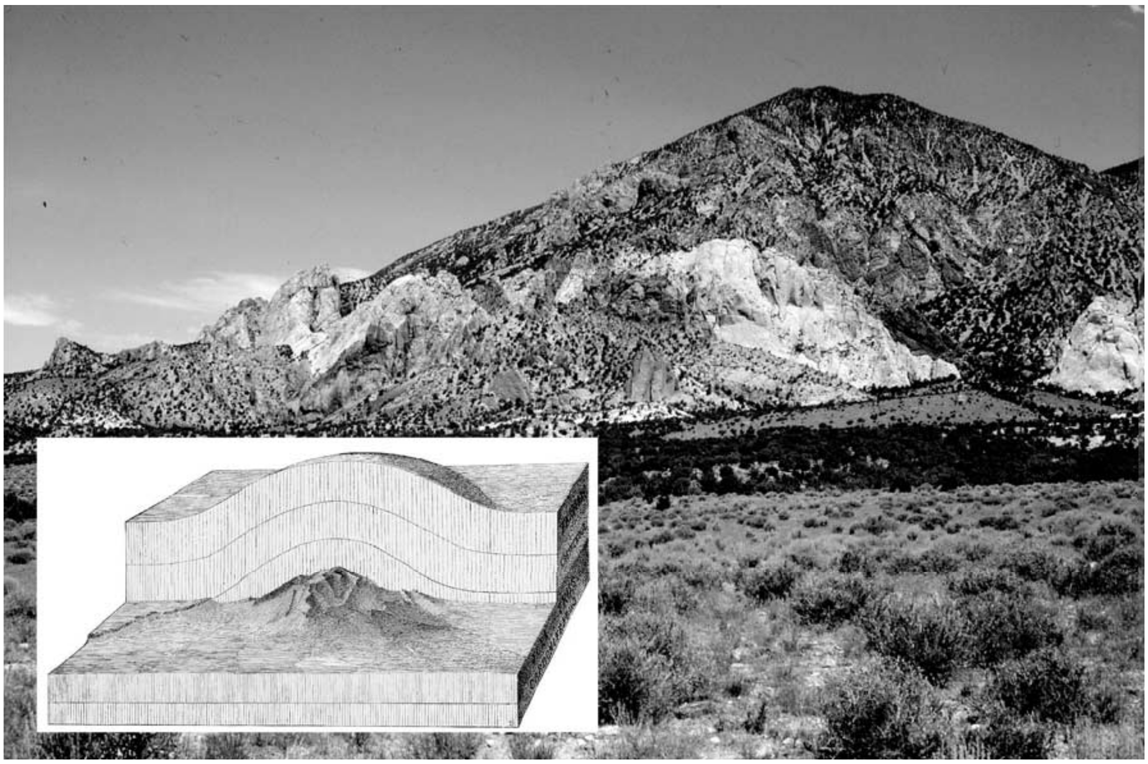

Mt. Hillers, southern Henry Mountains, UT. The mountain is cored by igneous rock and surrounded by upturned beds of sandstone and shale. G. K. Gilbert coined the term "laccolite" for these structures in the late 1870s and proposed models for this process of mountain building based on mechanical principles. Inset: Frontispiece from G. K. Gilbert's *Report on the Geology of the Henry Mountains* (Gilbert, 1877). To the rear of this illustration the sedimentary strata form the structural dome of Mt. Ellsworth, and to the front the eroded remnant of the dome represents the current topography of this mountain. Photograph by D. D. Pollard.

The sciences do not try to explain, they hardly even try to interpret, they mainly make models. By a model is meant a mathematical construct which, with the addition of certain verbal interpretations, describes observed phenomena. The justification of such a mathematical construct is solely and precisely that it is expected to work (quote from John von Neumann; Gleick, 1987, p. 273).

In this chapter we motivate the study of structural geology by introducing selected topics that illustrate the extraordinary breadth of interesting problems and important practical applications of this discipline. For example, we use the Imperial Valley earthquake of 1979 along the San Andreas Fault zone to describe techniques for geological hazard analysis. In a second example the lineaments visible in radar images of Venus provide the data for investigating tectonic processes on a planet other than our own. This is followed by an investigation of normal faulting in a hydrocarbon reservoir under the North Sea, off the coast of Norway, to introduce an application to petroleum exploration and production. Then we describe the pattern of small faults, veins, and solution surfaces from an exposure in southern France, an example that demonstrates the practice of structural geology at the human scale. The concept of "anticracks" that emerged from this academic investigation is now being used to help explain the origin of huge earthquakes a hundred kilometers below Earth's surface. Finally, we describe a mechanism for mountain building that was discovered in the Henry Mountains of southern Utah in the late nineteenth century by one of the pioneers of structural geology, G. K. Gilbert.

The frontispiece for this chapter is a photograph of Mt. Hillers in the southern Henry Mountains. Like all the photographs that appear as grayscale images in this book, a color image of this photograph is available at the textbook website along with images of related exposures and scenes. These are presented as monitor resolution images for quick viewing with a web browser or for LCD projection in the classroom for teaching purposes.

1.1 Earthquake hazards in southern California

Academic researchers have learned that society may not be content to continue funding the arcane studies of ancient rocks that have been the mainstay of the National Science Foundation's Tectonics Program in the past. Darrel Cowan, then President of the Geological Society of America's Structural Geology and Tectonic Division, concluded:

> We are at the end of the era when an unquestioning public belief in the benefits of basic scientific research almost automatically led to increased budgets at the NSF (National Science Foundation) Program level. Already, NSF management and the Congress want to hear arguments about how research, and especially new programs, will address important social issues: environmental changes and hazards, exploitation, waste, and recycling of natural resources, and the like (Cowan, 1992).

Thus, whether a career in the Earth sciences takes one to industry or to academia or to a government laboratory, the structural geologist should know how to address problems of social importance. To this end, we integrate aspects of active tectonics, engineering geology, and petroleum geology into this book to show how structural geology can contribute to solving problems in these areas.

Most inhabitants of southern California are familiar with earthquakes and the geological hazard associated with living in an active tectonic province, although the recurrence time of major events is great enough to instill a sense of complacency in many citizens. On the other hand, Earth scientists and government officials are acutely aware that destructive earthquakes could occur at any moment. Teams of scientists and engineers supported by federal and local governments are monitoring the continuing activity of the faults in this area and have tools in place to capture data from the next significant event (Yeats *et al.*, 1997).

What are the data that these scientists and engineers are hoping to capture? Perhaps the most fundamental aspect of faulting is the fact that the rock and soil on either side of the fault slip past one another. There is relative motion of these two masses more or less parallel to the fault surface. For example, Fig. 1.1 is a photograph taken across the trace of the Imperial Fault in the Imperial Valley of southern California shortly after a magnitude 6.5 earthquake struck on October 15, 1979. The vertical surface just behind the observer's feet is one surface of the fault exposed at the time of the earthquake. Relative to the ground on which the observer is standing, slip on the fault offset the two small drainage channels upward and to the right. By identifying soil particles (say in the bottom of the drainage channel) that were adjacent before the slip, one can make precise measurements of the offset. Using a tape measure, the geologist records the horizontal, *strike slip* component of relative motion as about 5 cm, and the upward, *dip slip* component as about 20 cm.

To characterize the behavior of a fault, one would like to know the magnitudes and directions of this relative motion in terms of the displacements, velocities, and accelerations of originally adjacent particles over the entire fault. The relative motion of particles is directly measurable only at (or very near) the surface of the Earth for active faults, and yet the fault might extend to depths of 10 km or more. Furthermore, one would like to know the distributions of these quantities over the entire time the two surfaces of the fault were in relative motion. In other words one would like to know the spatial and temporal distributions of displacement, velocity, and acceleration for particles of rock or soil in the vicinity of the fault. Given such information we could begin to understand the mechanisms that control fault slip and, perhaps, be in a position to be predictive about such events.

Fig 1.1 Ground rupture along the northern trace of the Imperial Fault in southern California after the October 15, 1979, magnitude 6.5 earthquake. View is to the southwest. The strike and dip components of slip are identified based on the offsets of the small stream channels. The relative motion is right-lateral strike slip (~5 cm) and dip slip (~20 cm) down to the northeast. See website for color image. Photograph by D. D. Pollard.

1.1.1 Contributions from geology, geodesy, and geophysics

Figure 1.2 is a schematic illustration of some of the tools used to monitor the slip across faults in active tectonic regions (Thatcher and Bonilla, 1989). The illustration in Fig. 1.2a represents a vertical cross section along the fault with contours of slip magnitude. The tools used to estimate the *slip distribution* fall within three different disciplines in the Earth sciences: namely geology, geodesy, and geophysics. The geologist measures the offset of geological structures and formations across a fault at the surface as well as the offset of whatever cultural markers might be present (Fig. 1.2b). By walking along the surface trace of the fault, the structural geologist can gather data on many different types of geological and cultural features and plot a graph of fault slip at the surface versus distance along the fault. Usually the geologist records only the total slip between a time before the earthquake and a time after the earthquake, and cannot measure the velocities or accelerations that occurred during the slip event.

Although the data gathered by geologists provide the most direct measurement of slip at the Earth's surface, they only record the slip at certain points along the fault and these data may not be similar to the distribution of slip at depth. For example, the offset of a fence line at the surface may be strongly influenced by a thick layer of relatively soft soil or unconsolidated sediments overlying the more rigid rock below. Models are required to interpolate the surface slip between these data points and to extrapolate these surface measurements to the sub-surface. Using elasticity theory, one could specify remote stresses and stresses along the fault as boundary conditions and solve for the slip distribution over the fault surface. One could search for boundary conditions that produced a slip distribution best matching the slip measured at the surface. Of course the model parameters themselves may be poorly constrained, and there may be many possible slip distributions at depth that are consistent with data from the surface. None-the-less, such modeling exercises are the only way for the geologist to extrapolate data from the surface to the sub-surface.

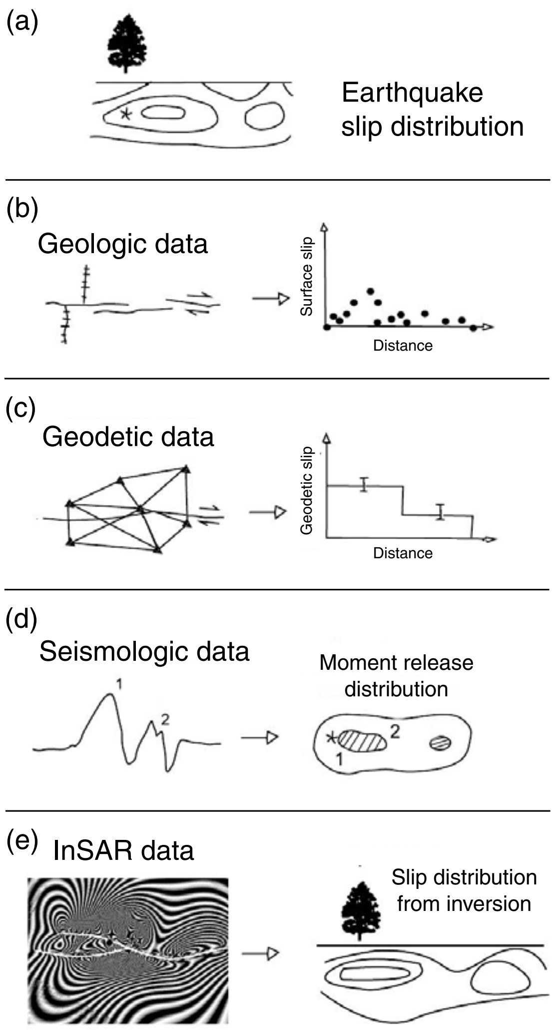

Fig 1.2 Schematic diagram of four different methods for estimating the slip on a fault (Thatcher and Bonilla, 1989). The actual slip is contoured on the fault surface in (a). Illustrations (b)–(d) show how geologists, geodesists, and seismologists gather data (left column), and graphical representations of these data are shown to the right. (e) Interferometric synthetic aperture radar (InSAR) data provide the field of displacement at the surface near a fault which can be inverted to estimate the slip distribution.

The geodesist measures the changes in lengths, angles, and/or elevations between surveyed benchmarks usually located at scattered points some distance from the fault (Fig. 1.2c). Such measurements are often more precise than geological measurements because high-precision instruments are used to gather the data and the bench marks are fixed to carefully designed and stable monuments. In some cases the instruments are permanently mounted at the survey locations and record data that can be used to calculate velocities and accelerations. In these respects the geodetic data can provide a better constraint on the deformation associated with faulting.

On the other hand the benchmarks usually are not located at the fault itself, so they do not directly record fault slip, even at the surface. Rather, a model (usually based on elasticity theory) is employed that requires as input the location and geometry of the fault and the mechanical behavior of the rock mass underlying the geodetic network. These models usually treat the fault as a set of segments, each with a constant slip, so the output is slip at the surface for different segments of the fault (Fig. 1.2c). The geodetically inferred slip is consistent with the changes in line lengths or angles between the benchmarks of the array, but clearly depends upon the chosen segment geometry and the other model parameters. More elaborate models are capable of calculating slip distributions at depth from the geodetic data. Because the geodetic data come from widely scattered locations away from the fault, the geometry and mechanical behavior of the sub-surface materials over a large volume of rock must be provided as model input.

The third category of data is taken from seismograms recorded both in the vicinity of the fault and at distant stations at the time of the earthquake (Fig. 1.2d). Although the locations of the seismographs may be even more remote from the fault than the geodetic benchmarks, these instruments continuously record the shaking of the ground due to the passage of *seismic waves* generated at the fault. Therefore, they can provide a wealth of data for inferring the behavior of the fault. In this example pulses on the seismogram are correlated to areas on the fault at depth that slipped at slightly different times or at different distances from the recording instrument. What is actually calculated is the *seismic moment* on the fault over these areas, but this can, in principle, be related to the average slip. By combining data from many seismographs a picture of the moment release distribution on the fault can be constructed. In practice the instruments may not be ideally located, and there may not be as many as one would desire.

Models of the sub-surface fault geometry are needed as well as the mechanical properties (seismic wave velocities) of the rock from the fault to the location of the seismographs.

The use of interferometric synthetic aperture radar (InSAR) for the detection of ground displacements associated with earthquakes was highlighted in articles appearing in the early 1990s (Massonnet *et al.*, 1993; Prescott, 1993; Zebker *et al.*, 1994). The radar signal is transmitted from a satellite to the ground surface where it is reflected back to the satellite and recorded as a set of pixels making up an image of the surface. Knowledge of the travel time and speed of the signal provide the information necessary to calculate the range, or distance, from the satellite to each reflective site on the surface. If the same region is imaged at two different times, for example before and after the earthquake, the difference between the two images can be used to calculate the component of the surface displacement directed toward the satellite. The resulting image (Fig. 1.2e), called an *interferogram*, is similar to a contour map of the displacement component on which the white and black bands (called fringes) are the contours. The fault segments are shown as fine white lines superimposed on this image. By invoking a model (usually based on elasticity theory) for the location and geometry of the fault segments and the mechanical behavior of the rock mass, one may use this displacement distribution on Earth's surface to calculate the corresponding slip distribution on the fault. The abundance of data provides considerable constraint on the unknown slip distribution below Earth's surface and very exciting avenues for new research on faulting.

It should be obvious from this discussion that the different disciplines contribute information that is based on different observations in different locations and over different length and time scales. Yet scientists from all three disciplines are studying the same physical phenomenon, faulting, and they are using the same tools to build their models, namely elasticity theory. In this textbook we focus on the geological data and the models that are used to relate measurements of slip to fault behavior. On the other hand each discipline is providing important pieces of the puzzle, so structural geologists should be aware of the concepts and contributions from geophysics and geodesy to the study of faulting. In addition important insights are attained from studying the effects of faulting on the geomorphology of the landscape (Arrowsmith *et al.*, 1996; Arrowsmith *et al.*, 1998). The most comprehensive view of faults and the faulting process will come from an integration of all these data and that integration will be most effective in the context of building well-constrained models.

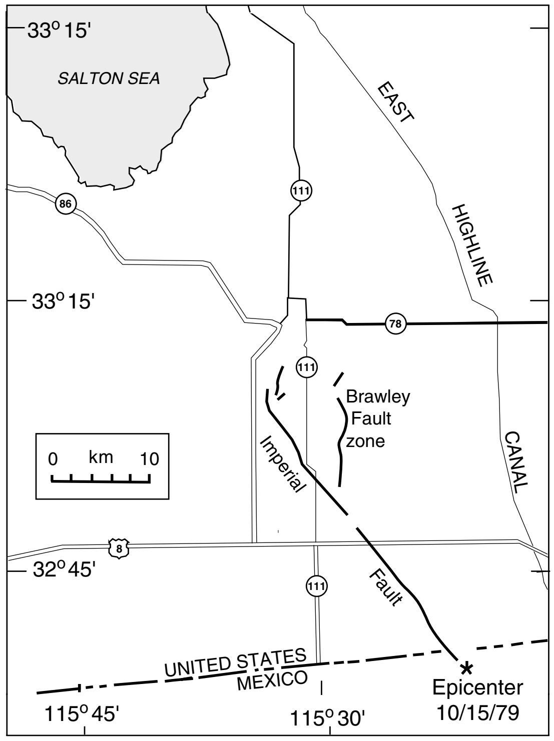

Fig 1.3 Map of the region affected by the October 15, 1979, earthquake in southern California (Wosser *et al.*, 1982). The epicenter is shown as a star in the lower right-hand corner.

1.1.2 Conceptual and mechanical models for the 1979 earthquake rupture

On October 15, 1979, the magnitude 6.5 earthquake rupture began just south of the US–Mexico border and spread approximately 35 km to the north into southern California (Fig. 1.3), breaking ground along the trace of the Imperial Fault (Johnson *et al.*, 1982; Wosser *et al.*, 1982). Many agricultural features such as fence lines and canals provided markers to measure the slip

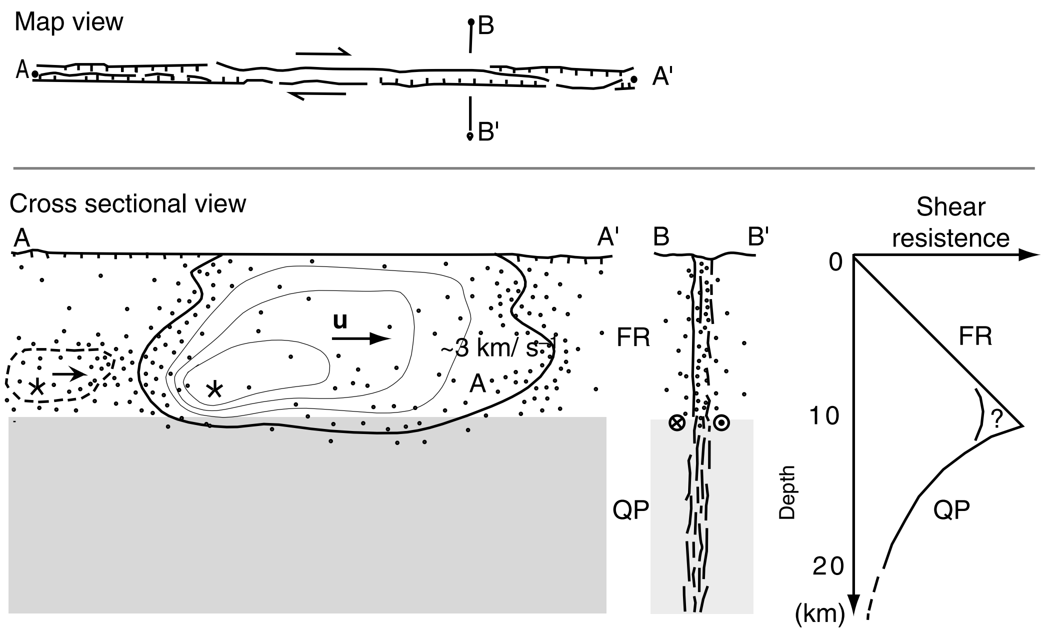

Fig 1.4 Three views of a crustal-scale strike slip fault. Map view illustrates the fault as a zone of deformation. Cross section A–A′ in the fault plane includes a contour map of the slip (**u**) which goes to zero at the fault tipline and is greatest near the hypocenter (star). Cross section B–B′ perpendicular to the fault plane suggests that slip mechanisms are frictional resistance (FR) in the upper part of the crust and localized quasi-plastic flow (QP) in the lower part. The graph at the right indicates a linearly increasing resistance to shearing with depth to the brittle–ductile transition, and then a non-linear decreasing resistance to shearing with depth. Reprinted from Sibson (1989) with permission from Elsevier.

across the fault trace. The farmers, homeowners, businesses, and municipalities in the Imperial Valley, mostly around the town of El Centro, sustained over twenty million dollars in damage. Fortunately, there was no loss of life and few catastrophic failures of man-made structures in this event. On the other hand, earthquakes of similar magnitude often are accompanied by many deaths in regions with less stringent building codes, or no building codes at all. These events testify to the destructive power of earthquakes and to the need to understand such hazards. Because earthquakes are generated by sudden slip on faults, we need to understand the mechanisms and behaviors of faults in order to develop informed hazard mitigation policy. Just what are the causes and consequences of dynamic rupture on faults? Some answers to this question have come from research by scientists and engineers over the past few decades, but much remains to be understood.

In the previous section we described how geologists, geodesists, and geophysicists use models to extrapolate information on displacements or accelerations from the locations where data are measured on the Earth's surface to the fault in the sub-surface. These models help us to understand the behavior of faults where they cannot be observed directly and they provide insights concerning earthquake faulting as a structural process. The faulting process is conceptualized at the crustal scale in Fig. 1.4 for a vertical fault with strike slip motion (Sibson, 1989). Each view of this conceptual fault model reveals different aspects of faulting at the crustal scale. The map view shows a zone of fractures and deformation, rather than two surfaces in contact. This suggests that faults can be more complex than a single fracture and that shearing of material in a fault zone may characterize the deformation rather than slip between two surfaces. The vertical cross section viewed parallel to the fault indicates that frictional resistance (labeled "FR" in Fig. 1.4) to slip on a fault operates to depths of perhaps 10 km and plastic flow (labeled "QP") is associated with distributed shearing in a zone at deeper levels. Thus, the mechanisms of faulting may change with depth as temperature and pressure increase, such that brittle fracture and friction dominate at shallow depths and ductile flow dominates at greater depths. In this conceptual model the resistance to shearing increases with depth to this transition and then decreases with depth. In a vertical section viewed perpendicular to the fault (A–A′), dynamic shearing begins at depth, near the *brittle–ductile transition* and spreads out over the fault surface at a velocity of about 3 km s^{-1}, eventually reaching the Earth's surface.

The Imperial Valley earthquake is noteworthy because it occurred within a dense array of geodetic and geophysical instruments and there were abundant cultural features for the geologists to measure at the surface (Savage *et al.*, 1979). The mechanical model reviewed here was constructed using data from the seismographs and strong motion instruments that monitored this event (Archuleta, 1984). The results are not unique and the choice of model parameters could be debated, but that is not the issue here. This model provides an excellent example of the insight one can gain about phenomena that are otherwise totally inaccessible to direct observation.

Figure 1.5a is a map of the rupture traces for both the Imperial and Brawley Faults as compiled by geologists from observations at the Earth's surface. The photograph shown in Fig. 1.1 was taken near the northern end of the Imperial Fault. The map also shows rupture traces along the Brawley Fault that trend oblique to the Imperial Fault. Apparently the Brawley Fault slipped at about the same time as the Imperial Fault, but the relative motion on the Brawley Fault was primarily dip slip. Note that the southern half of the Imperial Fault rupture trace is drawn as continuous, whereas it is drawn as composed of discrete segments in the northern half. Also shown on Fig. 1.5a is the rupture *epicenter*, the point at the surface of the Earth immediately above the point where rupture initiated, as inferred by geophysicists from seismic records. This location is dependent upon a model for the seismic wave velocities of the crustal rocks. Note that the epicenter was approximately 5 km south of the southernmost surface break.

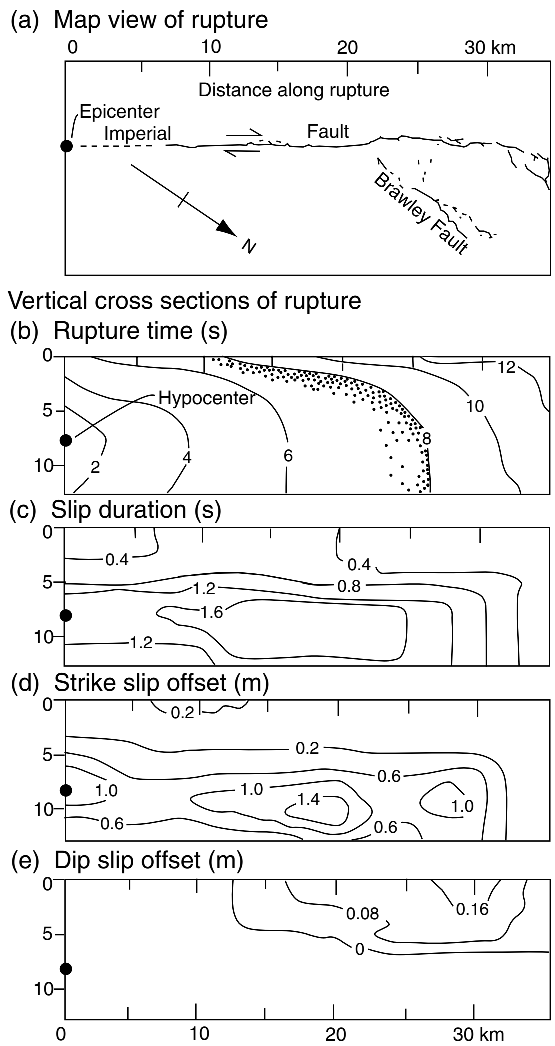

Fig 1.5 Map and cross sections of the Imperial Fault and the Brawley Fault for the October 15, 1979, earthquake in southern California (Archuleta, 1984): (a) map of the rupture trace; (b)–(e) vertical cross sections parallel to the fault trace with contours of the model rupture time, slip duration, strike slip offset, and dip slip offset.

Each of the observations made in the previous paragraph brings up interesting questions about faulting. Why did the rupture not break to the surface immediately over the epicenter? Why would a second fault rupture at the same time as the Imperial Fault, and why is the trace of the second fault obliquely oriented? What does the discontinuous nature of the rupture trace tell us about faulting? Some of these questions can be addressed with models for the rupture process.

The mechanical model for the October 15, 1979, earthquake event considers only the rupture along the Imperial Fault (Archuleta, 1984). The lower four panels of Fig. 1.5 are graphs of different physical quantities calculated using the model and plotted on a vertical planar section that approximates the more complex geometry of the actual fault as suggested by the mapped trace in the first panel. The model fault is about 12 km in depth (ordinate) and 35 km in length (abscissa). The physical quantities (rupture time, slip duration, strike slip, and dip slip) are represented by contours of equal magnitude on these graphs. Together these panels provide a remarkable visualization of the model slip event from the Earth's surface to the bottom of the rupture.

Figure 1.5b illustrates the position of the leading edge of the model rupture to the north of the point of rupture initiation, the *hypocenter*, at times measured in seconds after initiation. What happened to the south of the hypocenter is ignored on these panels. At a given time, say 4 s, that portion of the fault between the hypocenter and the 4-s contour has slipped, while elsewhere on the fault no slip has occurred. Clearly, slip on the model fault does not initiate everywhere simultaneously. Rather, the model rupture initiated at a point, at the hypocentral depth of about 8 km. Then, the rupture front advanced rapidly to the north and less rapidly upward toward the surface. The rupture took a total time of about 12 s to spread the 35 km to the north end of the model fault. Thus, the average *rupture velocity* was about $3\,\mathrm{km\,s^{-1}}$ toward the north, approximately the speed of seismic shear waves.

Figure 1.5c shows the total time that originally adjacent particles on the two surfaces of the model fault were in relative motion. For example, along the contour labeled "1.6 s" the two surfaces slipped for a total time of less than 2 s. You might find this surprising given the fact that the total duration of faulting was about 12 s. Clearly all parts of the model fault were not slipping at the same time. This is illustrated in the previous panel by the pattern of dots next to the 8-s contour. These dots cover the relatively small portion of the fault that has already slipped and is still in the process of slipping at the moment that the rupture front lies along the 8-s contour. Between these dots and the hypocenter the model fault has slipped and stopped, whereas to the north and above the 8-s contour the fault has not yet slipped. At any particular location on the model fault the slipping occurred over a period of time ranging from a fraction of a second to almost 2 s as the rupture front passed, and then slipping stopped.

Figures 1.5d and e show, respectively, two components of slip between the model fault surfaces after the rupture has completed its propagation from the hypocenter to the northern termination. Strike slip varies from 1.4 m near the bottom center of the fault to a few decimeters or less at the surface. The strike slip is zero along the southern portion of the fault at the surface and this is consistent with the observations shown on the map in the first panel. Note that the surface measurements of slip, amounting to about 20 cm, under-represent the slip at depth by a factor of eight or more. The model fault slipped much more at depth than at the surface. Dip slip is concentrated near the surface at the northern end of the model fault with magnitudes approaching a few decimeters. This is consistent with the geological observations (see Fig. 1.1) that indicate the rocks on the northeastern side of this part of the Imperial Fault went down relative to those on the southwestern side. The amount of dip slip at the surface (up to about 20 cm) also is consistent with the field observations. The relative motion on the Brawley Fault was also nearly pure dip slip with the northwestern side down. In fact, the region between the Imperial and Brawley Faults is a topographic depression occupied by a (usually) dry lake-bed. This suggests that the relative motion experienced during the 1979 earthquake is typical of the recent geological history of this fault system.

This mechanical model gives us a picture of active faulting that is reasonably consistent with the available surficial and seismic data from the 1979 event. It informs our intuition about the physical process of faulting and provides a glimpse into possible behavior along the Imperial Fault at depth. Building models such as this one and using these models to understand the process of faulting is an exciting area of research in which structural geologists can participate (Segall and Pollard, 1980; Aydin and Schultz, 1990; Cowie and

Scholz, 1992; Dawers *et al.*, 1993; Bürgmann *et al.*, 1994; Muller *et al.*, 2003).

1.2 Radar lineaments on Venus

In his book *The Assayer* Galileo Galilei apparently wrote the following:

> The Universe, which stands continually open to our gaze, cannot be understood unless one first learns to comprehend the language and read the letters in which it is composed. It is written in the language of mathematics . . . (Gregory, 1990).

Today the power of modern telescopes and satellite exploration of the planets provides countless opportunities to investigate structures in rock beyond Earth.

The Magellan mission to Venus produced radar images of much of the planet's surface and many of the structures observed on these images apparently are related to volcanism (Head *et al.*, 1992). One of the most interesting classes of structures is composed of radar *lineaments* (paired bright and dark lines or single bright lines on the image) that appear to radiate from a central focal point like spokes on a bicycle wheel (Fig. 1.6). Grosfils and Head (1994) have identified more than 160 such radial systems on Venus and have interpreted the lineaments as fractures cutting the surface of the Venusian crust. At first glance the patterns are reminiscent of radial fracture patterns you might have seen in a pane of tempered glass where it has been struck by a rock; however, these lineament patterns are enormous. The pattern at (15°S, 215°E), shown in more detail in Fig. 1.7, is about 200 km in diameter and the average diameter for all such patterns identified on Venus is 325 km, with some as great as 2000 km! These patterns are intriguing in their symmetry and awe inspiring in their size; they clearly warrant our attention as structural geologists.

Grosfils and Head (1994) developed conceptual models to distinguish and interpret two types of radial lineament patterns. For the first type they suggest the fractures are formed by doming and stretching of the Venusian crust over a body of molten rock, *magma*, that flows upward from a source reservoir at depth. The fractures themselves are not filled with magma; rather they are the ephemeral manifestation of a large rising body of magma beneath the surface. The second type of lineament pattern is interpreted as having formed as magma-filled fractures, *dikes*, that propagated upward and radially outward from a central magma conduit at shallow depths under the volcanic edifice. The dikes act as the passageways for magma flow to the surface from the central conduit. Here we only consider the second type, which apparently makes up more than 70% of the radial patterns identified on Venus.

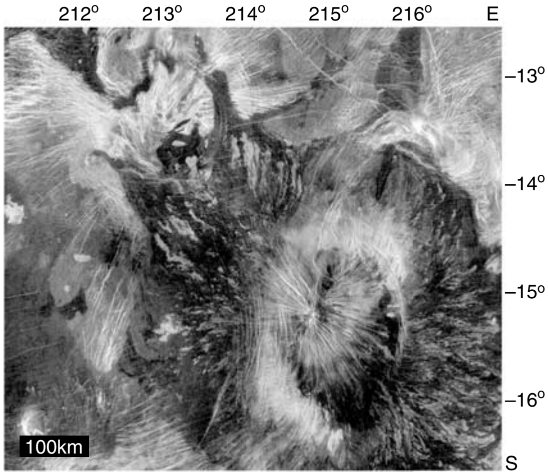

Fig 1.6 Left-looking F-MIDR 15s214 radar image of the surface of Venus from the Magellan mission (Koenig and Pollard, 1998). Look angle is approximately 40°. Note radial pattern of lineaments centered at 15°S, 215°E. One degree of latitude or longitude is about 100 km.

1.2.1 Conceptual and mechanical models for graben formation

The volcanic edifice at (15°S, 215°E) stands about 1 km above the surrounding plains. Elongate and lobate gray regions (labeled "rlf" on Fig. 1.7) on the surface of this edifice are interpreted as lava flows (Koenig and Pollard, 1998), which spread down the flanks of this large volcano before solidifying. Also visible on the radar image are paired radial bright and dark lines that extend up to 50 km down the slope (labeled "g" on Fig. 1.7). These are interpreted as *graben*, linear depressions about 1 to 2 km in width bounded by normal faults along which the central block of rock has moved downward. When obliquely incident radar signals are

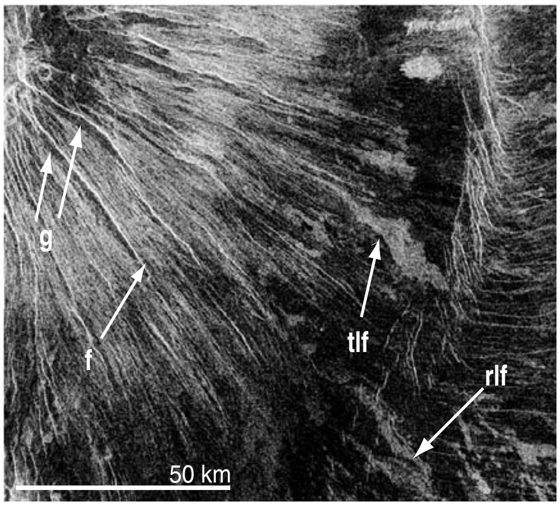

Fig 1.7 Left-looking F-MIDR 15s214 radar image of the southeast quadrant of the volcanic edifice centered at 15°S, 215°E. Surface structures are identified (Koenig and Pollard, 1998) as graben (g), fractures (f), terminal lava flows (tlf), and radial lava flows (rlf). The graben and fractures radiate from the volcanic center in the upper left corner of the image.

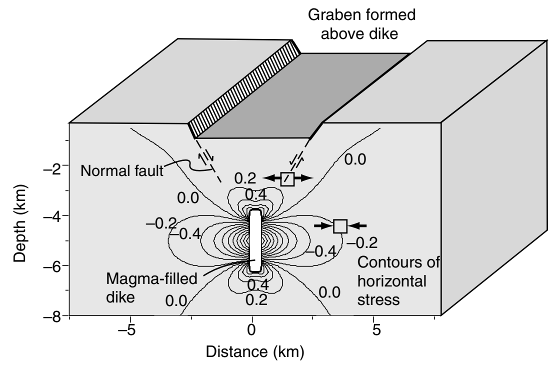

Fig 1.8 Schematic block diagram of a graben bounded by two normal faults and underlain by a dike (Rubin and Pollard, 1988; Koenig and Pollard, 1998). The horizontal stress component induced by opening of the dike is contoured on the front view showing a stress shadow (negative, compressive stress) to either side of the dike and a stress concentration (positive, tensile stress) near the dike tips.

reflected off the fault surface on one side of the graben, returning a bright lineament, the fault surface on the other side of the graben lies in a radar shadow and forms a dark lineament. Thus the surface topography accounts for the closely spaced pairs of bright and dark lines on the image.

Figure 1.8 illustrates the conceptual model for the development of graben over igneous dikes. The pairs of normal faults bounding graben on Venus are interpreted as having formed because of the local horizontal stretching of the rock immediately over or ahead of vertical dikes. Because the dikes apparently propagated upward and outward from a central magma chamber located under the summit of the edifice at (15°S, 215°E), the graben form a radial pattern on the flanks of this volcano.

A couple of questions come to mind when thinking about the origin of graben as described in the previous paragraph. Does the opening of a dike actually lead to stretching at the surface? If it does, why should two normal faults form to either side of the dike instead of one immediately over the dike? These questions have been addressed by studying the physical relationships between normal faults and dikes (Rubin and Pollard, 1988; Rubin, 1990). Horizontal stretching is caused by tensile stresses that tend to pull the rock apart. Therefore, one needs to determine if dike opening at depth could induce tensile stresses near the Earth's surface, where normal faults bound the graben. Such associations are found in volcanic regions on Earth, including those in Iceland and Afar.

The mechanical model of this phenomenon is based on principles that are formulated into a set of mathematical equations known as the *theory of elasticity* (Timoshenko and Goodier, 1970). This theory and the relevant equations are described in detail later in this textbook. For the moment you only need to know that these equations can, for example, be solved to determine the stress distribution in the rock mass surrounding a dike. This formulation is called a *boundary value problem* because one prescribes the stresses on the boundaries of a body and the governing equations of elasticity theory are used to calculate the stresses in the interior. In this case one boundary represents Earth's surface, which is free of stress, and the other boundaries represent the dike walls that are subjected to stresses equal to the outward-directed pressure of the magma. The magma pressure pushes the dike walls apart and distorts the surrounding rock mass, thereby inducing a change in the stress distribution that is not easy to imagine without the aid of elasticity theory.